

Compact High-Redshift Galaxies Are the Cores of Present-Day Massive Spheroids

Philip F. Hopkins^{1*}, Kevin Bundy¹, Norman Murray^{2,3}, Eliot Quataert¹, Tod Lauer⁴, Chung-Pei Ma¹

¹*Department of Astronomy, University of California Berkeley, Berkeley, CA 94720*

²*Canadian Institute for Theoretical Astrophysics, 60 St. George Street, University of Toronto, ON M5S 3H8, Canada*

³*Canada Research Chair in Astrophysics*

⁴*National Optical Astronomy Observatory, Tucson, AZ 85726*

Submitted to MNRAS, March 3, 2009

ABSTRACT

Observations suggest that the effective radii of high-redshift massive spheroids are as much as a factor ~ 6 smaller than low-redshift galaxies of comparable mass. Given the apparent absence of low-redshift counterparts, this has often been interpreted as indicating that the high density, compact red galaxies must be “puffed up” by some mechanism. We compare the ensemble of high-redshift observations with large samples of well-observed low-redshift ellipticals. At the same physical radii, the stellar surface mass densities of low and high-redshift systems are comparable. Moreover, the abundance of high surface density material at low redshift is comparable to or larger than that observed at $z > 1 - 2$, consistent with the continuous buildup of spheroids over this time. The entire population of compact, high-redshift red galaxies may be the progenitors of the high-density cores of present-day ellipticals, with no need for a decrease in stellar density from $z = 2$ to $z = 0$. The primary difference between low and high-redshift systems is thus the observed low-density material at large radii in low-redshift spheroids (rather than the high-density material in high-redshift spheroids). Such low-density material may either (1) assemble at $z < 2$ or (2) be present, but not yet detected, at $z > 2$. Mock observations of low-redshift massive systems show that the high-redshift observations do not yet probe sufficiently low surface brightness material to detect the low surface density “wings” (if present). Thus, if the high-redshift galaxies resemble the most massive systems today, their inferred effective radii could be under-estimated by factors $\sim 2 - 4$. This difference arises because massive systems at low redshift are not well-fit by single Sérsic profiles. We discuss the implications of our results for physical models of galaxy evolution.

Key words: galaxies: formation — galaxies: evolution — galaxies: active — galaxies: ellipticals — cosmology: theory

1 INTRODUCTION

Recent observations suggest that high-redshift spheroids may have significantly smaller effective radii than low-redshift analogues of the same mass (e.g. Daddi et al. 2005; McIntosh et al. 2005; Trujillo et al. 2006a; Zirm et al. 2007; Toft et al. 2007; van Dokkum et al. 2008; Franx et al. 2008; van der Wel et al. 2008; Cimatti et al. 2008). The apparent differences are dramatic: the inferred effective radii are as much as a factor ~ 6 smaller at fixed stellar mass in the most massive galaxies at $z = 2$. Whatever process explains this apparent evolution must be particular to this class of galaxies: disk galaxies are not similarly compact at high redshift

(Ravindranath et al. 2004; Ferguson et al. 2004; Somerville et al. 2008). As such, these observations represent a strong constraint on models of galaxy and bulge formation.

Relative to the abundance of massive galaxies today, there are not a large number of compact systems at high redshift. However, even if just $\sim 10\%$ survived intact to $z = 0$, this would greatly exceed the observed number density of such systems in the local Universe (Trujillo et al. 2009). In fact, at fixed stellar mass, ellipticals with older stellar populations appear to have the largest radii (Gallazzi et al. 2006; Bernardi et al. 2007; Graves et al. 2009).

The challenge for both observations and models is therefore to understand how these high-redshift systems could evolve to become “typical” spheroids today. Their masses, number densities, and clustering dictate that they are the progenitors of the most mas-

* E-mail: phopkins@astro.berkeley.edu

sive ellipticals and BCGs today (Quadri et al. 2007; Hopkins et al. 2007c). These systems have much larger R_e and thus have lower effective densities $\Sigma_{\text{eff}} = M_*/(<R_e)/(\pi R_e^2)$. However, this does not necessarily mean that the physical densities are lower than those of the high-redshift systems. One way to increase R_e would be to uniformly “puff up” the profiles, lowering the physical density everywhere. This would imply that the central densities of massive high-redshift ellipticals would need to decrease by two orders of magnitude from $z = 2$ to $z = 0$. Alternatively, R_e can change by just as much by adding a relatively small amount of mass at low surface densities and large radii, without affecting the central density at all. In other words, an evolving effective density does not necessarily imply an evolving physical density at all radii.

Buildup of an “envelope” of low-density material is expected as massive early-forming galaxies undergo late-time (major and minor) gas-poor mergers with later-forming, less-dense ellipticals, disks, and dwarfs (Gallagher & Ostriker 1972; Ostriker & Tremaine 1975; Hausman & Ostriker 1978; Weil & Hernquist 1994, 1996; Naab et al. 2007). This is a relatively efficient channel for size-mass evolution, yielding factor of several size evolution with only a factor 1.5 – 2 increase in stellar mass (Hopkins et al. 2008d). But this less dense material added at large radii does not significantly affect the high-density core,¹ and so these models predict that the dense, high-redshift systems should survive to become the central regions of (some fraction of) today’s massive ellipticals.

If, on the other hand, high-redshift systems evolved primarily by equal-mass dry mergers between equivalently dense spheroids, then this will “inflate” the profiles relatively uniformly. In this extreme case, effective radii and stellar mass both approximately double in the merger; high-redshift systems would be uniformly more dense than their low-redshift descendants (see e.g. Hernquist et al. 1993; Boylan-Kolchin et al. 2006).

Distinguishing between these possibilities, as well as other dynamical, stellar evolution, or observational effects that could lead to apparent size-mass evolution clearly depends on understanding in detail differences in the surface density profiles of spheroids as a function of radius, at low and high redshift. In this paper, we quantitatively compare low and high-redshift observations to constrain these scenarios and inform how systems are evolving from $z \gtrsim 2$ to $z \sim 0$.

In § 2 we directly compare the observed profiles of high and low-redshift massive spheroids, and show that, at the same physical radii, their stellar surface mass densities are comparable. The massive, high redshift systems appear no different than the “cores” of today’s massive ellipticals. In § 3 we determine the distribution of maximum/central densities, and show that this has not evolved significantly from $z = 0$ to $z > 2$. In § 4 we calculate the mass function (and global mass density) of these high-density “cores” at both low and high redshift. This allows us to quantitatively compare the abundance of high-density material observed at both low and high redshifts. We show that there is as much or more high-density material in the cores of massive spheroids at $z = 0$ as is observed to be in place at $z = 1 - 2$. The difference between low and high-redshift systems, we conclude, lies in the lack of observed low surface-density envelopes around the high-redshift systems. In § 5 we show that, although it is certainly possible that such en-

velopes do not exist at high redshifts, it is premature to rule them out: observations do not yet reach sufficiently low surface brightness limits. Specifically, we show that if the high-redshift systems had identical profiles to their low-redshift analogues, similar small sizes would be recovered from high-redshift observations, given that low-redshift systems are not intrinsically true Sersic profiles. We summarize our results and discuss their consequences for physical models of spheroid evolution in § 6.

Throughout, we assume a WMAP5 cosmology ($\Omega_M = 0.27$, $\Omega_\Lambda = 0.73$, $h = 0.705$; Komatsu et al. 2008), but the exact choice makes no significant difference.

2 SURFACE DENSITY PROFILES OF ELLIPTICALS AT HIGH AND LOW REDSHIFT

Figure 1 shows a direct comparison of the observed surface stellar density profiles of high-redshift compact galaxies and low-redshift massive galaxies. At low redshift we compile observed surface brightness profiles from Kormendy et al. (2008) and Lauer et al. (2007); this consists of a total of ~ 180 unique local ellipticals with nuclear *HST* observations and ground-based data at large radii (allowing accurate surface brightness profile measurements from ~ 10 pc to ~ 50 kpc).² The isophotally averaged major axis profiles are measured in rest-frame optical; we convert to a stellar mass profile based on the measured total stellar masses and the assumption of a radius-independent stellar mass-to-light ratio. Conversion to stellar mass profiles using e.g. color or stellar population gradients and comparison of profiles from different instruments and wavebands in these samples are discussed extensively in Hopkins et al. (2008a,b); the differences are much smaller than the scatter between individual profiles, and do not affect our conclusions. In Figure 1, we restrict our comparison to massive galaxies with $M_* > 10^{11} M_\odot$ ³ because these systems are most likely to be descendants of massive high-redshift galaxies. The Kormendy et al. (2008) sample is a volume-limited survey of the Virgo spheroid population; as such it includes few very massive galaxies ($M_* > 3 \times 10^{11} M_\odot$). The Lauer et al. (2007) galaxies are chosen to be representative of massive ellipticals in the local Universe, including more massive systems up to a couple $10^{12} M_\odot$. At the masses of interest, both are representative of the distribution of spheroid sizes in the local SDSS galaxy sample (Shen et al. 2003).

Figure 1 compares the low-redshift sample with the observed, PSF de-convolved profiles of nine high-redshift compact massive galaxies ($M_* \gtrsim 10^{11} M_\odot$, $R_e \sim 1$ kpc), specifically the $z \sim 2 - 3$ sample from van Dokkum et al. (2008). This is a well-studied sample that represents the extreme of implied size evolution: the inferred average R_e is a factor of ~ 6 smaller than local spheroids of the same mass. Figure 1 shows the best-fit Sersic profile of each galaxy in the sample; stellar mass-to-light ratios are determined

¹ By “core,” we refer to the central regions of the galaxy, not to any specific class of central profile slopes. We use the phrases “cusp ellipticals” or “core ellipticals” to distinguish these.

² Note that although the composite (HST+ground-based) profiles were used in Lauer et al. (2007) to estimate effective radii, they were not actually shown in the paper.

³ Stellar masses for all objects are determined from the combination of rest-frame optical and near-IR photometry, corrected to an assumed Chabrier (2003) IMF. We refer to Hopkins et al. (2008a) and Kriek et al. (2008b) for details of the low and high-redshift samples, respectively. Varying the specific bands used to determine stellar masses makes little difference, and changing the IMF will systematically change the stellar masses of all objects considered, but will not change our comparisons.

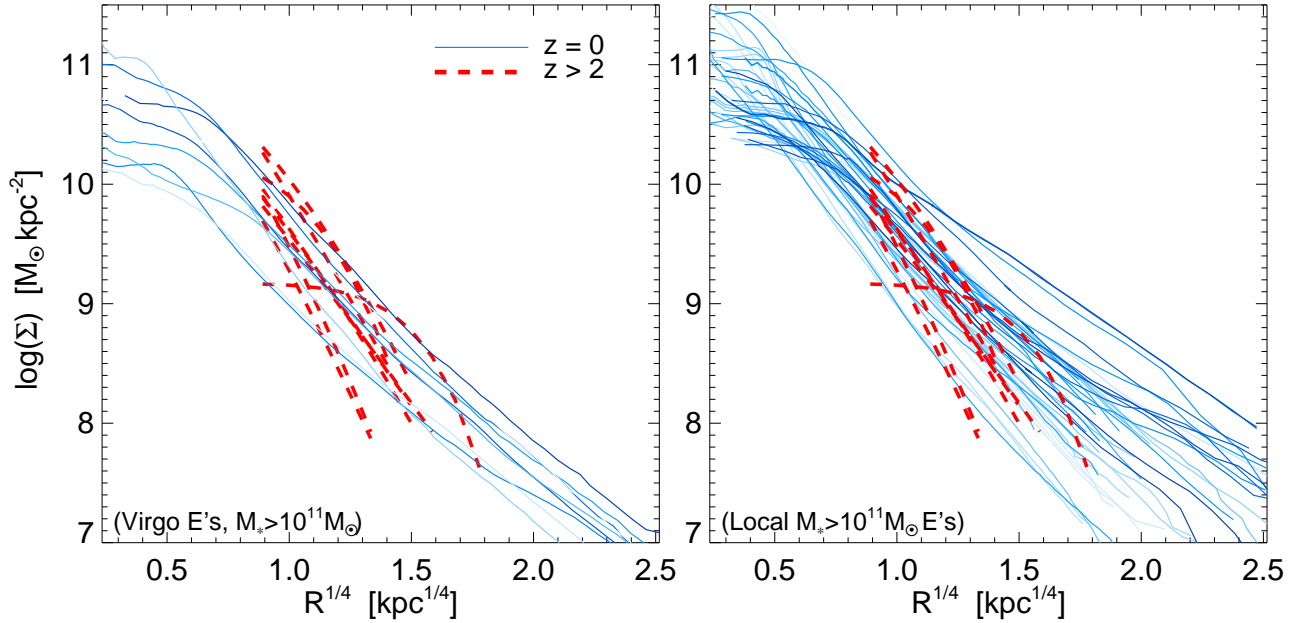


Figure 1. Direct comparison of the (major axis) surface stellar mass density profiles of $z \gtrsim 2$ compact massive spheroids ($M_* \sim 10^{11} M_\odot$, best-fit $R_e \sim \text{kpc}$; red dashed) and local, massive ellipticals ($M_* \geq 10^{11} M_\odot$, $R_e \gtrsim 4 - 5 \text{ kpc}$; solid). Both Σ and R are in physical units. The high- z profiles are the PSF de-convolved fit, plotted over the observed range in radius given the best-case limitations in seeing and surface brightness (from van Dokkum et al. 2008). The low- z profiles combine space and ground-based photometry to obtain very large dynamic range; they are from the Kormendy et al. (2008) Virgo elliptical sample (left) and the Lauer et al. (2007) local massive elliptical sample (right). The former is a volume-limited sample, so contains fewer very massive galaxies with high central surface brightness. Although the high- z systems have much smaller R_e , their densities at any physical radius are not unusual compared to the local objects: the central $\sim 1 - 2 \text{ kpc}$ of massive ellipticals today are just as dense. The difference in R_e owes to the presence of the large wings/envelopes at low surface density in the low-redshift objects.

by assuming a radius-independent M_*/L and normalizing the observed portion of the profile to the total stellar mass determined from photometry and spectroscopy in Kriek et al. (2006, 2008b,a). We plot the profile of each system over the maximum radial range observed: from the scale of a single pixel at the observed redshift to the limiting surface brightness depth of the best images. Both the low and high-redshift systems are plotted in terms of major-axis radii (a non-negligible correction).

At low redshift, the stellar mass-to-light ratios of ellipticals appear to be nearly independent of radius (reflected in e.g. their observed weak color gradients), but the stellar mass-to-light ratio may depend significantly on radius in the high-redshift systems (Trager et al. 2000; Côté et al. 2006; Sánchez-Blázquez et al. 2007). However, based on the observed stellar population gradients in local ellipticals, the observed ages/colors of the high-redshift systems, or the outcomes of numerical simulations, the expected variation in M_*/L is such that a young, recently-formed post-starburst stellar population at the center of the high-redshift galaxy will have higher L/M_* than older stars at larger R_e (see e.g. Hopkins et al. 2008c). This would make the high-redshift systems less dense than we assume here; we conservatively allow for the maximal stellar mass densities in those systems.

The comparison in Figure 1 is quite striking: although the best-fit effective radii and effective surface densities of the high-redshift systems are quite different from their low-redshift analogues, the actual stellar surface mass densities at any given observed radius do not appear significantly higher than a substantial fraction of the low-redshift population. In other words, inside the same observed radii $\sim 1 - 5 \text{ kpc}$, many of today’s massive ellipticals are just as dense as the high-redshift systems. The difference in

effective radius stems primarily from the fact that the low-redshift systems have substantial extended wings/envelopes of low surface-brightness material ($\Sigma \ll 10^9 M_\odot \text{ kpc}^{-2}$); by contrast, the inference from fitting the high-redshift systems is that their profiles fall more rapidly at large radii (as we discuss further below).

3 CENTRAL STELLAR DENSITIES

Figure 2 plots the *peak* surface stellar mass densities Σ_{peak} obtained in both the low and high-redshift galaxy populations. The “maximum” or peak surface density must be defined within some radius, for galaxies whose surface density continues to rise to unresolved radii (e.g. cusp ellipticals; although most of the local massive galaxies are core ellipticals, with relatively flat maximum surface densities within $\sim 50 - 500 \text{ pc}$). For example, the maximum stellar surface density can be defined as the average Σ interior to some fixed small radius $\sim 50 - 100 \text{ pc}$, or a fixed fraction of R_e from $\sim 0.02 - 0.04$, or by extrapolation to $R = 0$ of a best-fit Sérsic profile – we are simply interested in comparing the central densities at small radii in both low and high-redshift systems. For each determination, we find qualitatively similar results albeit with some small normalization differences; Figure 2 shows Σ_{peak} determined from averaging within 50 pc and within $0.02 R_e$. For the high-redshift systems, PSF and seeing effects smear out the maximum observed surface brightness/density inside $\sim 1 \text{ kpc}$; we extrapolate the best-fit Sérsic profiles inwards to the same radii as the local systems. Making this same approximation in the low-redshift samples shows that it is reasonable, but tends to slightly over-estimate the central surface density, especially in core ellipticals.

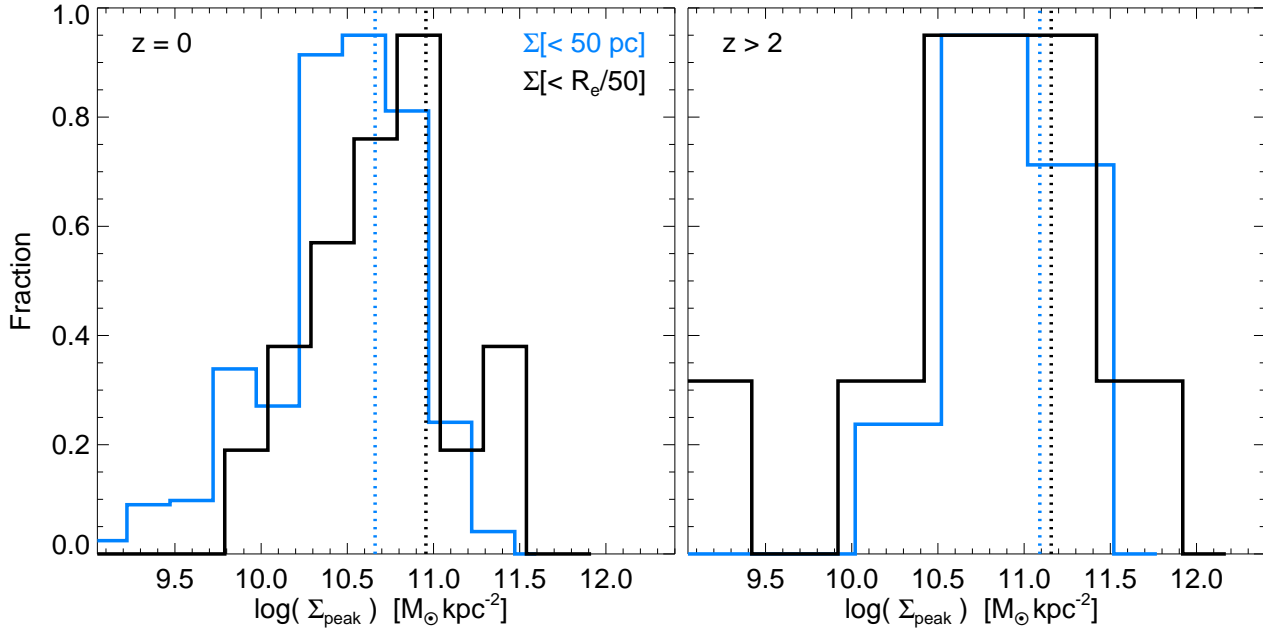


Figure 2. Distribution of peak (maximum) spheroid stellar mass surface densities. *Left:* Low- z systems from Figure 1. Most ellipticals, at any mass, have $\Sigma_{\text{peak}} \sim 0.3 - 1 \times 10^{11} M_{\odot} \text{ kpc}^{-2}$. Histograms show two different calculations of Σ_{peak} (within 50 pc and $R_e/50$); dotted lines are the median from each. *Right:* Same, for the high- z samples. Direct observations are PSF and seeing-limited, so we extrapolate the best-fit Sersic profile inwards to obtain Σ_{peak} (this is typically an upper limit in the low- z samples). The results are striking: central densities are reasonably independent of redshift.

At both low and high redshift, there is a characteristic maximum central surface stellar mass density $\sim 0.3 - 2 \times 10^{11} M_{\odot} \text{ kpc}^{-2}$, with significant, but still surprisingly little scatter given the known diversity in the profile shapes of ellipticals (e.g. variation in Sersic indices and cusp versus core populations). The maximum surface density of the high-redshift systems is perhaps a factor ~ 2 larger than that of low-redshift systems, but given that we are extrapolating Sersic profiles inwards for the high-redshift systems, this is probably an upper limit. Thus while the observations imply up to a factor ~ 40 evolution in effective surface brightness, there is nowhere near this much evolution in the true maximum stellar surface density, a much more physically relevant quantity.

It is worth noting that the mass and redshift-independence in Σ_{peak} in Figure 2 is somewhat surprising, given the diversity of formation histories and scatter in e.g. the mass present at larger radii (see e.g. Hopkins et al. 2009d). A more detailed discussion of this will be the subject of future work, but it may relate to the maximum surface density of gas that can turn into stars (see § 6).

4 THE MASS AT HIGH STELLAR DENSITIES

We now quantify the amount of mass at different stellar surface densities. In order to reduce the effects of noise and PSF effects (important in particular for the high-redshift systems), we define the surface density in this section as the average surface density within each radius, i.e. $\Sigma(R) = \langle \Sigma(< R) \rangle = M_*(< R) / \pi R^2$. We obtain similar results using the local Σ , but with larger noise. For each observed system in our low-redshift sample, given the stellar mass profile (Figure 1), we calculate the total fraction of the stellar mass that lies above a given threshold in surface density Σ_{min} . We evaluate this for each system separately, and in Figure 3 we plot the average mass fraction at each Σ for all observed systems in our sample, in several bins of total stellar mass. Although the mass

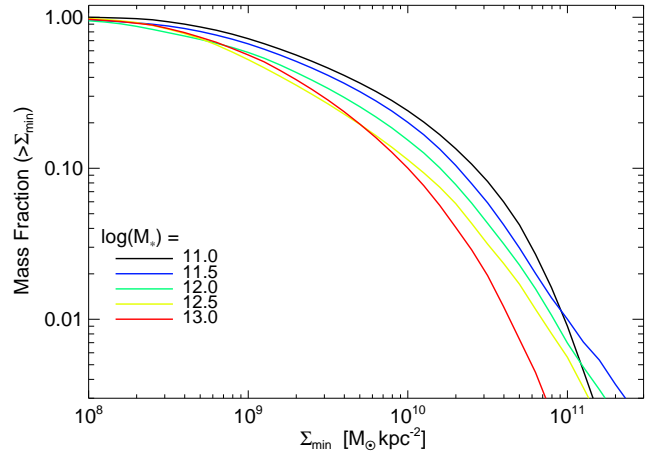


Figure 3. Average mass fraction above some threshold surface stellar mass density Σ_{min} , for the low- z sample from Figure 1. The values shown are the average fraction of *all* spheroid mass (in a narrow range around each M_*) above the given Σ_{min} . A significant fraction of the $z = 0$ spheroid mass ($\sim 25\%$) resides in matter at the inferred effective Σ of the high- z compact systems ($10^{10} M_{\odot} \text{ kpc}^{-2}$).

fraction above each Σ_{min} can vary by a large amount from galaxy to galaxy, the average is surprisingly robust across masses (and does not depend significantly on whether we include both cusp and core ellipticals or evaluate the two separately). By sufficiently low Σ_{min} thresholds, $\sim 10^8 M_{\odot} \text{ kpc}^{-2}$, essentially all mass in spheroids is accounted for; some systems have more extended, lower surface-brightness envelopes, but they contribute little total mass. Approximately $\sim 25\%$ of the stellar mass density at each mass remains above $\sim 10^{10} M_{\odot} \text{ kpc}^{-2}$ – a typical effective surface brightness for high-redshift ellipticals – in moderately high-mass systems (dropping to $\sim 10\%$ by the most massive $10^{13} M_{\odot}$ systems). By a thresh-

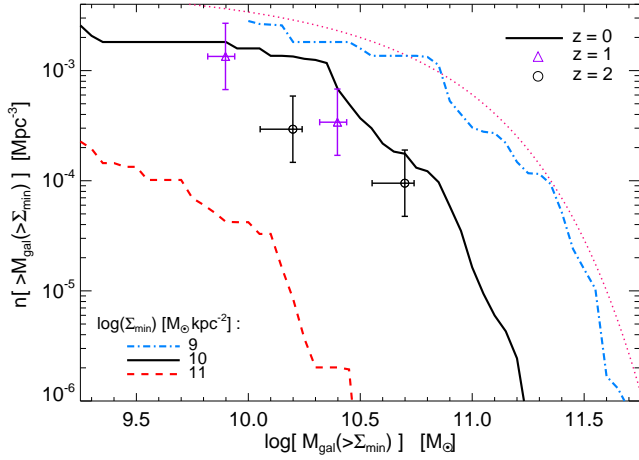


Figure 4. Spheroid stellar mass function (number density) for mass above a given surface stellar mass density threshold (Σ_{\min}). We calculate the $z = 0$ mass function of spheroids including *only* stellar material in any galaxy above the given Σ_{\min} , given the total stellar mass function and the observed distribution of profile shapes. The magenta dotted line shows the total spheroid mass function (Bell et al. 2003) – most of the mass is accounted for above $10^9 M_{\odot} \text{ kpc}^{-2}$. The value of $\Sigma_{\min} = 10^{10} M_{\odot} \text{ kpc}^{-2}$ corresponds to the effective surface density of the compact high-redshift spheroids; points show the results of the same calculation for the observed high-redshift systems and this value of Σ_{\min} . We show this for the $z \sim 2.3$ data from van Dokkum et al. (2008, black circles) and $z \sim 1$ data from van der Wel et al. (2008, triangles).

old of $\sim 10^{11} M_{\odot} \text{ kpc}^{-2}$, we have reached the maximum/peak surface densities of ellipticals (Figure 2), and the mass fractions at higher densities drop rapidly.

The best-fit Sérsic profiles of the $z \sim 2$ systems imply that they have higher mass *fractions* above a high surface density threshold $\sim 10^{10} M_{\odot} \text{ kpc}^{-2}$. However, as illustrated above, this primarily owes to their having less mass at low Σ , not more at high Σ .

The comparison between the low and high-redshift samples can be made more quantitative by determining the stellar mass function above a given surface density threshold. To do so, we ignore all stellar mass in the Universe below a given threshold in Σ , and construct the spheroid mass function. The mass of a given galaxy is only the mass above that Σ ; i.e. we calculate the volumetric number density of spheroids with $\Sigma > \Sigma_{\min}$

$$n[>M_{\text{gal}}(>\Sigma_{\min})] \equiv \frac{dN(\text{galaxies}|M_i > M_{\text{gal}})}{dV} \quad (1)$$

as a function of the integrated mass above Σ_{\min} ,

$$M_i \equiv M(>\Sigma_{\min}) = \int_{\Sigma=\Sigma_{\min}}^{\Sigma \rightarrow \infty} \Sigma \times 2\pi r dr. \quad (2)$$

The resulting mass functions are shown in Figure 4. In detail, we take the observed stellar mass function of spheroids (Bell et al. 2003), and at each mass, convolve with the distribution of surface density profiles from Kormendy et al. (2008) and Lauer et al. (2007) for systems of the same mass, to determine the resulting mass function (number density) above a given surface density threshold.⁴ We are assuming that the distribution of profile shapes

⁴ Note that “density” here has two meanings: the volume density (the y-axis of Figure 4) is the total number of galaxies meeting a given criteria per unit volume; the surface density is the local stellar surface mass density of stars within a particular galaxy.

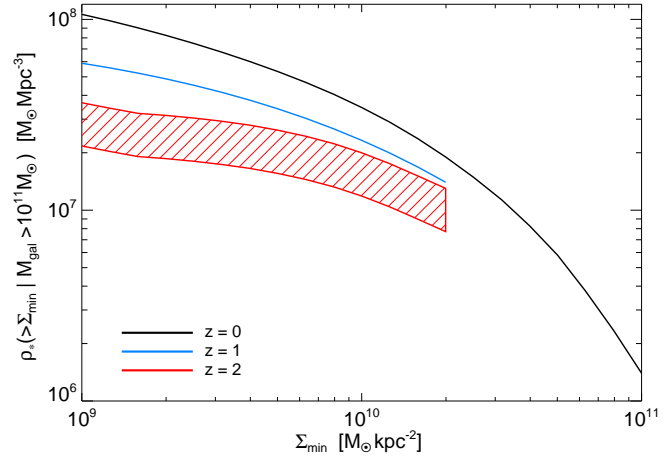


Figure 5. The total global mass density of stars which reside in massive galaxies (total galaxy mass $> 10^{11} M_{\odot}$) and are above a threshold stellar mass surface density (within the galaxy) of Σ_{\min} . This is the integral of Figure 4, including only massive galaxies. We show the results from observations at $z = 0$ (black), $z = 1$ (blue) and $z = 2$ (red; shaded range corresponds to typical uncertainties in the total mass density of these compact high- z systems). The high- z data is limited to the highest Σ directly observed (limited by resolution and seeing). At $z = 0$, $\sim 4 \times 10^7 M_{\odot} \text{ Mpc}^{-3}$ is locked in massive ellipticals above a surface density of $> 10^{10} M_{\odot} \text{ kpc}^{-2}$. This is a factor of a few larger than the mass density at such Σ at $z \sim 2$.

in Kormendy et al. (2008) and Lauer et al. (2007) are representative at each mass. Their sample selection as well as other measurements (see those works and e.g. Trujillo et al. 2002; Ferrarese et al. 2006; Allen et al. 2006) and the close agreement in fundamental plane correlations and Sérsic index distributions in larger volumes (e.g. Shen et al. 2003) suggest that this is probably a good assumption.

Unsurprisingly, Figure 4 shows that at lower Σ thresholds the predicted mass function converges to the total stellar mass function of spheroids, i.e. most stellar mass is accounted for. And at high thresholds it drops rapidly, especially at high masses: $10^{11} M_{\odot} \text{ kpc}^{-2}$ is the peak surface density inside $\ll 1 \text{ kpc}$ at both low and high redshifts – no observed systems have significant amounts of mass $> 10^{11} M_{\odot}$ above this threshold.

In Figure 4 we compare the $z = 0$ volume density of mass at $\Sigma > 10^{10} M_{\odot} \text{ kpc}^{-2}$ (solid lines) with observational inferences at $z = 1$ (diamonds) and $z = 2$ (circles). Specifically, given the *total* number density of $> 10^{10} M_{\odot}$ spheroids/compact red systems at these redshifts (Pérez-González et al. 2008), convolved with the distribution of profile shapes from van Dokkum et al. (2008), we obtain the number density of objects with mass above the relevant Σ threshold. In the error budget in Figure 4, we include the difference in number densities estimated by Fontana et al. (2006), van Dokkum et al. (2006), and Marchesini et al. (2008), and variation in the distribution of profile shapes/sizes fitted in other works, including Trujillo et al. (2007); Toft et al. (2007); Buitrago et al. (2008); Cimatti et al. (2008). These yield similar conclusions to within a factor $\sim 2 - 3$. At the masses of interest, the observations should be reasonably complete to these high surface densities.

We can also integrate the mass functions in Figure 4 to obtain the total volume density of stellar mass in spheroids above some threshold in surface density Σ_{\min} ; this is shown in Figure 5. Whereas mergers will not conserve number density, they should conserve total stellar mass in this calculation (to the extent that they do not change the Σ_{\min} of the central regions of galaxies). Since the high-redshift systems are primarily massive, $> 10^{11} M_{\odot}$, and their

descendants cannot presumably be much lower mass, we restrict this calculation to only systems with a *total* stellar mass above this limit (although this only removes the very lowest-mass contributions to the high- Σ population in Figure 4, and does not substantially affect our comparison). We then calculate, in systems above this mass, the total stellar mass above each threshold Σ_{\min} .

Figure 5 shows that there is $\sim 4 \times 10^7 M_{\odot} \text{Mpc}^{-3}$ of stellar mass in $> 10^{11} M_{\odot}$ ellipticals, above a surface density threshold of $\Sigma > 10^{10} M_{\odot} \text{kpc}^{-2}$ in the local Universe. This is comparable to the *total* stellar mass density of high-redshift red spheroids (Labbé et al. 2005; van Dokkum et al. 2006; Grazian et al. 2007; Abraham et al. 2007). Convolving over the observed size distribution at $z \sim 2$, the mass density above this threshold Σ is of course lower $\sim 1 - 2 \times 10^7 M_{\odot} \text{Mpc}^{-3}$. We obtain a similar result comparing to the $z = 1$ observations from van der Wel et al. (2008), with the relevant constraints being at lower surface density as there is less relative evolution.

Our comparisons indicate that the local Universe contains just as much, or more, stellar mass at high surface densities as implied by observations of high-redshift systems. It is thus possible that all of the high-stellar mass density systems at high redshift can be incorporated into massive ellipticals today, without any conflict with their observed number densities or surface brightness profiles. In fact, a reasonable amount of high-surface density material must continue to be added to the elliptical population, perhaps by gas-rich mergers, from high redshifts until $z = 0$. It is the subject of another study whether gas-rich mergers produce an adequate amount of high- Σ stellar mass in current galaxy formation models to account for the observed growth of ρ_* in Figure 5. Nonetheless, the high density material at high redshifts is not inconsistent with the $z \sim 0$ data and therefore does not have to “go away.”

5 THE MASS AT LOW STELLAR DENSITIES

Our results demonstrate that the difference between low and high-redshift spheroids does not arise in their central densities, but in the large envelopes of low surface brightness material observed in low-redshift systems. This is the origin of their larger effective radii.

There are two natural ways of reconciling the low and high-redshift observations with the hypothesis that the high-redshift spheroids are the progenitors of today’s ellipticals. First, the high-redshift systems may not have much low-density material at large radii; low-density material would then have to be accreted at lower redshifts via late-time mergers (minor or major) with gas-poor disks and ellipticals (i.e. lower-density systems). Such a scenario is feasible – if the initial spheroid-forming mergers are sufficiently gas-rich, there will be little low-density material from extended stellar disks to contribute to an extended envelope (Hopkins et al. 2008a). And comparison of clustering properties, merger rates, and stellar populations all imply that these massive, high redshift systems *should* grow by a factor $\sim 1.5 - 2$ via these channels between $z \sim 2$ and $z = 0$, more or less sufficient to account for the envelopes seen in Figure 1 (see e.g. van Dokkum 2005; Bell et al. 2006; Zheng et al. 2007; Lin et al. 2008; Conroy & Wechsler 2008).

The second way of reconciling the low and high-redshift observations is that high-redshift systems do have material at low surface densities already, but it is not seen in present observations.

Figure 6 illustrates circumstances under which the high-redshift observations may not be sensitive to extended, low- Σ wings. We consider a few representative galaxy profiles from the local sample of Kormendy et al. (2008), ranging from low-mass

cusp ellipticals with low Sersic indices at large radii (steep surface density falloff), to high-mass core ellipticals with high Sersic indices at large radii (extended envelopes).⁵ For each, we convolve the observed profile with a simple Gaussian PSF with typical best-case resolution for the high-redshift observations of interest ($1\sigma = 0.5 \text{ kpc}$; FWHM 1.2 kpc). We then fit the profile, in a manner mimicking observations, to a *single* Sersic profile (fitting appropriately convolved model profiles). We do this as a function of image depth. Specifically we plot the results of the fits as a function of $\Delta\mu \equiv \mu_{\max} - \mu_{\min}$, the surface brightness (mag arcsec^{-2}) of the deepest point included relative to the central/maximum surface brightness of the convolved image. In Figure 6 we plot the resulting best-fit effective radii, considering both fits with a free Sersic index n_s and a fixed $n_s = 4$. For fits with a free n_s , we plot the corresponding best-fit n_s .

For low-mass galaxies, which have low n_s and therefore fall off steeply in Σ at large R , the true profiles can be recovered with even relatively shallow observations. If anything, for the lowest mass-galaxies, which have Sersic profile indices $n_s \sim 2 - 3$ (when fit in this manner to a single Sersic index; see e.g. Balcells et al. 2007b,a; Ferrarese et al. 2006), the effects of the PSF tend to slightly *increase* the inferred effective radius in shallow images. For systems very close to $n_s = 4$, characteristic of intermediate-mass galaxies, there is almost no depth-dependent bias to the inferred R_e and n_s (see NGC 4515 in Figure 6). The same conclusions are reached in the analysis of mock-redshifted SDSS images of low-mass galaxies in van der Wel et al. (2008).

However, for systems with larger outer Sersic indices, indicative of more extended envelopes and characteristic of massive galaxies, the inferred R_e and n_s become increasingly sensitive to image depth. Considering the entire sample, we find that the typical depth required to obtain a “converged” R_e and n_s (to within $\sim 30 - 50\%$ of the value obtained with the deepest available data) is a strong function of stellar mass, rising from $\Delta\mu \sim 4 \text{ mag}$ in intermediate-mass systems to $\Delta\mu \sim 6 - 8$ in high-mass ($M_* > 10^{11} M_{\odot}$) systems. If we require that at least 50% of local systems have converged R_e , we obtain the approximate mass-dependent criteria $\Delta\mu_{\text{conv}} > 3.0 + 2.3 \log(M_*/10^{11} M_{\odot})$; if we raise our desired threshold to $\sim 75 - 90\%$, the minimum $\Delta\mu$ should be uniformly deeper by another 1.5 mag . In terms of physical radii, depth of $\Delta\mu \sim 4 \text{ mag}$ corresponds roughly to a maximum well-sampled, high S/N physical radius of $\sim 5 \text{ kpc}$; the depth required for obtaining converged R_e in massive systems ($6 - 8 \text{ mag}$) corresponds to physical radii $\gtrsim 20 - 50 \text{ kpc}$.

These criteria can be compared to the deepest available observations at $z \sim 1 - 2$, spanning $\Delta\mu \sim 3 - 4 \text{ mag}$ (S/N rapidly decreasing at $R \gg 5 \text{ kpc}$; see Trujillo et al. 2004; Cimatti et al. 2008; Damjanov et al. 2008). At these depths, our comparisons suggest

⁵ The specific five galaxies shown are (from top to bottom) NGC 4464, NGC 4515, NGC 4473, NGC 4365, and NGC 4552. The first three are classified as cusp ellipticals, the latter two as core ellipticals. The observations are described in Kormendy et al. (2008), but typically include $\sim 80 - 100$ photometric points from a few pc to $\sim 50 \text{ kpc}$ in radii; photometric errors are $\lesssim 0.04 \text{ mag arcsec}^{-2}$ (not visible in Figure 6). They have stellar masses of $M_* = (0.17, 0.13, 1.2, 3.9, 2.0) \times 10^{11} M_{\odot}$, true effective radii – fit from the full data with proper multi-component profiles – of $R_e = (0.60, 1.05, 3.19, 14.6, 10.6) \text{ kpc}$, and central velocity dispersions of $\sigma = (120, 90, 192, 271, 252) \text{ km s}^{-1}$. Fitting their *outer* profile shapes to Sersic profiles (where they are uncontaminated by the central, high surface-density components; see e.g. Hopkins et al. 2008a,d) yields best-fit outer Sersic indices of $n_s = (2.1, 3.9, 4.6, 7.1, 9.2)$.

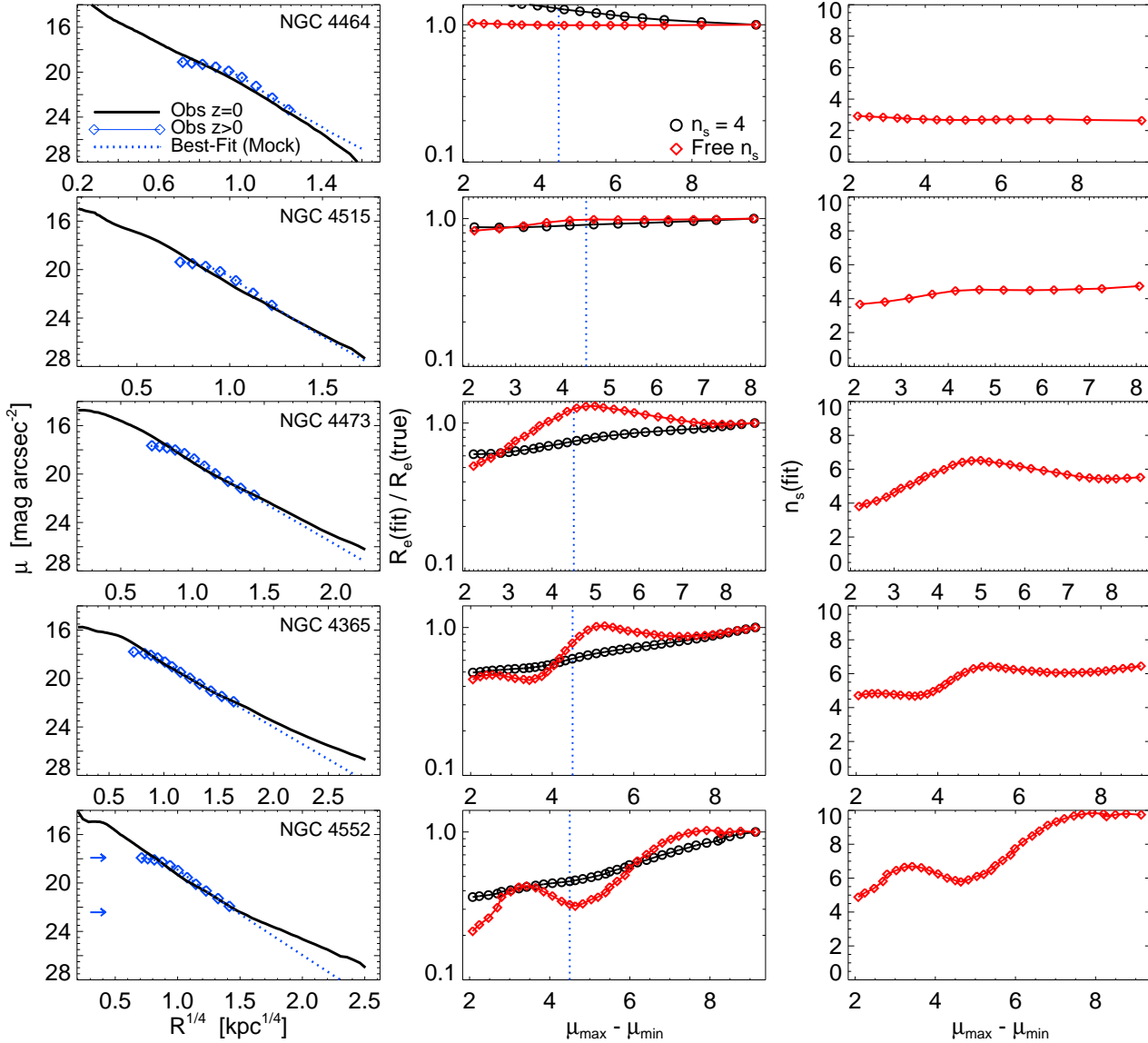


Figure 6. Best-fit light profile parameters R_e and n_s versus image depth. *Left:* Observed (V-band) surface brightness profiles (black) for several typical local spheroids in the Kormendy et al. (2008) sample,⁵ from low mass (low- n_s , i.e. steep light profile decay; *top*) to high mass (high- n_s , i.e. shallow decay/large envelope; *bottom*). These are compared to the profiles constructed from mock images of the same objects with best-case imaging available at $z \sim 0.5 - 2$ (cyan diamonds; seeing/PSF FWHM of 1.2 kpc, and depth/dynamic range of $\mu_{\max} - \mu_{\min} = 4.5$ mag; arrows in *bottom left*). Dotted cyan line shows the best-fit (convolved) Sersic profile fit to the mock high- z imaging data, extrapolated to large radii. *Center:* Effective radii of the best-fit Sersic profile, relative to the true R_e , as a function of image depth. We construct a series of mock profiles with similar PSF, seeing, noise, and pixel size (as *left*), but vary the image depth $\Delta\mu \equiv \mu_{\max} - \mu_{\min}$. We fit the resulting mock profile (with each $\Delta\mu$) with either a free Sersic index n_s (red diamonds) or fixed $n_s = 4$ (black squares). Dotted vertical line shows the $\Delta\mu$ of the mock profile at *left*. *Right:* Corresponding best-fit n_s (for free- n_s fits). At low masses (little stellar envelope), there is little dependence on the image depth. At high masses (large-envelope systems) a strong trend appears, because the $z = 0$ profiles of massive galaxies are fundamentally *not* well-described over a large dynamic range by single Sersic laws. At small $R \lesssim 2 - 10$ kpc ($\Delta\mu \sim 2 - 4$), the radii that dominate the fit in all but the deepest local imaging data, the profiles show a steeper falloff (indicative of $n_s \lesssim 4$, weak-envelope profiles) and yield a smaller best-fit R_e . Only at $R \gtrsim 20 - 50$ kpc ($\Delta\mu \sim 6 - 8$) do the low-density wings appear, leading to larger n_s and R_e .

that – if the “true” profiles were identical to those of today’s massive galaxies – R_e would be under-estimated by a factor $\sim 2 - 4$. Constructing mock images of the local systems matched to the spatial resolution and surface brightness limits of the observations at $z = 1$ and $z \sim 2.3$, and re-constructing the size-mass relation in each case in the same manner, we would recover a median fitted $R_e(1 - 3 \times 10^{11} M_\odot) \approx 2$ kpc, with a factor ~ 2 scatter (i.e., substantial numbers of galaxies with $R_e \sim 1$ kpc). These overall trends are similar to those observed.

These biases in inferred properties of high-mass galaxies arise

not just because they may have a substantial contribution from low surface brightness material at large radii (the envelope that disappears in shallow imaging). More fundamentally, it owes to the fact that such systems are *not* well-fit by single Sersic profiles. Indeed, it is now well-established that *no* populations of spheroids are well-fit by single Sersic profiles given sufficient dynamic range (see e.g. Kormendy 1999; Ferrarese et al. 2006; Lauer et al. 2007; Côté et al. 2007; Kormendy et al. 2008). As a consequence, although a single Sersic profile is often a formally good fit (in a χ^2 sense) over limited dynamic range, the best-fit n_s changes sys-

tematically as that dynamic range changes. The effect is most pronounced in the most massive galaxies. This is apparent in the example profiles in Figure 6. At small radii $R \lesssim 2 - 10$ kpc, systems are either “concave down” (which corresponds to a local Sersic index $n_s < 4$) or uncurved ($n_s = 4$). At larger radii, the profiles become more “concave up” ($n_s > 4$). High- n_s fits are due to the extended light, not the central regions. Moreover, the “central” regions relevant here extend to several kpc, and thus the effects are similar regardless of whether the system is a cusp or core elliptical.

It is important to stress that the mock observations fit the “correct” Sersic indices given the profile behavior over the observed dynamic range, but they do not sample the regime where the profile curvature changes form. As a result, our conclusion in Figure 6 that R_e may be underestimated by a factor $\sim 2 - 4$ in massive systems is in fact independent of the photometric details and fitting methodology; it more fundamentally reflects the fact that the surface density profiles of local massive systems change shape at large radii that are not probed in current observations of high-redshift systems. If, in fact, the high-mass systems shown in Figure 6 were perfect Sersic profiles, there would be little or no bias as a function of image depth (performing the same experiments on mock Sersic profiles suggests only $\sim 20\%$ bias at $\Delta\mu \sim 4$); since the profile shape at small radius would reflect this “true” n_s , the loss of the low-surface brightness features would not significantly affect the fits.

The fact that elliptical profiles may *not* be well-approximated as single Sersic profiles is important for interpreting the observations: a number of works have estimated that they are not biased in recovering the “true” R_e by constructing mock images of systems modeled as single Sersic profiles (e.g. Trujillo et al. 2006b, 2007; Cimatti et al. 2008). Others have tested their fits by mock-redshifting real systems, but the calibration samples have largely been low-mass, low- n_s systems (see e.g. the SDSS Virgo sample used in van der Wel et al. 2008). In these cases we do not expect any significant bias. However, the strongest claims of evolution in R_e are at the highest galaxy masses, where observed local galaxies are not well-fit by single Sersic profiles.

6 DISCUSSION

6.1 Can Yesterday’s Compact Spheroids Be the Cores of Today’s Ellipticals?

We have compared the stellar mass profiles of high-redshift, “compact” massive spheroids and well-studied local massive ellipticals. There has been considerable debate in the literature regarding the origins and fate of the compact high-redshift systems: they appear to be smaller ($R_e \sim 1$ kpc at $\sim 10^{11} M_\odot$) than all but a tiny fraction of local, similarly massive galaxies which have $R_e \sim 4 - 5$ kpc at $z = 0$. However, comparing the surface stellar mass density profiles directly, over the ranges that are actually well-sampled by observations, we show that the observed high-redshift systems have surface density profiles similar to the inner, dense regions of local massive ellipticals (Figure 1).

In other words, although the *effective* stellar mass surface density within R_e , $\Sigma_{\text{eff}} \equiv 1/2 M_*/(\pi R_e^2)$, is large in high-redshift systems, the physical stellar surface densities are comparable to the typical central surface densities observed at radii $\sim 0.5 - 5$ kpc in many local ellipticals. The centers or cores of local spheroids are just as dense as those of high-redshift systems: the difference is in the effective radii and effective densities, owing to the large, extended wings/envelopes of low surface brightness material around

local massive spheroids. This material leads to a larger R_e and lower effective surface density in the local systems.

We have further shown that the distributions of the *maximum* stellar surface densities are nearly the same at $z \sim 2$ and $z = 0$ (Figure 2) – at small radii today’s ellipticals have similar maximum nuclear stellar surface densities of $\sim 0.3 - 1 \times 10^{11} M_\odot \text{ kpc}^{-2}$ over a wide range in stellar mass from $\sim 10^9 M_\odot$ to $\gtrsim 10^{12} M_\odot$. The high redshift systems have their central surface densities smeared out by PSF and seeing effects, and thus do not reach these densities at any observed point; but extrapolating their best-fit Sersic profiles inwards they exhibit similar peak surface densities. High-redshift red galaxies are thus not uniformly more dense; indeed, the maximum/peak surface density of spheroids does not appear to evolve significantly from $z \gtrsim 2$ to $z \sim 0$.

Using a large sample of local, high-dynamic range observations, we have constructed a census of the local spheroid population and have quantitatively calculated the number of systems with central/core mass densities above a given surface mass density and stellar mass threshold (Figures 3-5). We have used this to construct the stellar mass function of spheroid “cores” – i.e. the stellar mass function of the parts of today’s ellipticals that lie above a given surface stellar mass density threshold.

The regime of particular interest is $\Sigma \sim 10^{10} M_\odot \text{ kpc}^{-2}$, which corresponds to the effective surface brightness of the high-redshift compact systems ($10^{11} M_\odot$ with $R_e = 1$ kpc). We find that $\sim 25 - 35\%$ of the stellar mass density in $z = 0$ massive spheroids lies above this surface density. Typical ellipticals have cores containing $\sim 1 - 5 \times 10^{10} M_\odot$ above this threshold. Comparing this to the observed properties of massive galaxies at $z = 1$ and $z = 2$, we find that by both number and total stellar mass, all of the high-redshift, compact systems can be accounted for in the cores of today’s ellipticals. For example, even in the extreme case in which every $z = 2$, $10^{11} M_\odot$ or larger spheroid (space density $\approx 10^{-4} \text{ Mpc}^{-3}$) had $R_e = 1$ kpc, this would correspond to the same space density of systems with $> 1/2 M_* = 5 \times 10^{10} M_\odot$ above the effective surface density $10^{10} M_\odot \text{ kpc}^{-2}$. At $z = 0$, the space density of such massive, high surface density cores is a factor $\sim 1.5 - 2$ higher. Doing the calculation more properly (convolving over the mass function and distribution of profile shapes), there is a factor ~ 2 more mass in local massive cores than is present at $z > 2$; the difference is qualitatively similar, but smaller, comparing to $z = 1$ populations. Not only can the high-redshift systems be accommodated (rather than being destroyed), but high density material in the centers of ellipticals may continue to build up even at relatively low redshifts.

6.2 How Does this Relate to Physical Models?

These conclusions are of considerable importance for physical models of spheroid formation and evolution, and in particular for the models that have been proposed to explain both the formation of high-redshift, apparently compact galaxies and their evolution into local $z = 0$ systems.

Models for spheroid formation naturally predict that ellipticals and bulges are fundamentally two-component objects, with a dense, central core built by dissipational processes – the loss of angular momentum in a progenitor gas disk, which then falls to the center and turns into stars in a compact starburst – and an extended, lower-density envelope build by dissipationless processes – the violent relaxation of progenitor disk stars, observed to be at much lower phase-space densities than the compact cores of ellipticals (Mihos & Hernquist 1994; Hopkins et al. 2008b). Observations in the local Universe have confirmed much of this picture

and made it increasingly robust (Kormendy 1999; Hibbard & Yun 1999; Rothberg & Joseph 2004; Kormendy et al. 2008). Indeed, simulations by several independent groups consistently find that it is not possible to make realistic ellipticals without the appropriate mix of these two components (Barnes & Hernquist 1996; Naab et al. 2006; Cox et al. 2006; Oñorbe et al. 2006; Jesseit et al. 2007; Burkert et al. 2008). As such, the existence of dense cores in spheroids at both low and high redshifts is a natural consequence of dissipational spheroid formation.

It is possible, if mergers are sufficiently gas-rich⁶, to build just the high-density core, and to add the envelope in relatively gas-poor mergers at later times. Given the gas-richness of high-redshift galaxies, some size evolution is naturally predicted in models, with high-redshift systems being more dominated by the dense, dissipational remnant (Khochfar & Silk 2006; Hopkins et al. 2009b).

The high-redshift observations represent an ideal opportunity to catch such cores “in formation” and strongly constrain their physical origin. Today, such cores are typically extremely old: ~ 10 Gyr. At high redshifts, however, they have ages $\lesssim 500$ Myr (Kriek et al. 2006). Understanding their stellar populations, metallicities, kinematics, and densities is critical to inform models of how dissipation builds the central regions of galaxies. There appears to be a natural link between the observed compact red galaxies and bright sub-millimeter galaxies, which are intense starbursts with consistent number densities (accounting for their short duty cycles) and physical sizes (Tacconi et al. 2006; Younger et al. 2007, 2008; Cimatti et al. 2008). This class of SMGs is widely believed to be the product of major mergers (Shapiro et al. 2008; Tacconi et al. 2008). Establishing further connections between these populations would not only enable new tests of the merger hypothesis, but would also rule out alternative models (e.g. monolithic collapse) for spheroid core formation.

The maximal mass densities of spheroids at both low and high redshift ($\sim 10^{11} M_{\odot} \text{ kpc}^{-2}$), for example, may inform models of star formation and feedback in extreme environments. This maximum surface density is intriguingly similar to previous suggestions of maximal (Eddington-limited) starbursts: if the observed mass surface density is initially pure gas, forming stars according to the Kennicutt (1998) relation (giving $\sim 2500 M_{\odot} \text{ yr}^{-1} \text{ kpc}^{-2}$), this implies a luminosity $= 1.5 \times 10^{13} L_{\odot} \text{ kpc}^{-2}$. This is the Eddington limit for dusty systems (Thompson et al. 2005). And, interestingly, it corresponds to the maximum SFR surface density in dense SMGs (Tacconi et al. 2006; Younger et al. 2008). The fact that so few ellipticals scatter above this peak surface density also suggests that their centers may have formed in a few dissipational events – if Eddington-limited arguments explain these peak densities, then there is no reason why they could not be exceeded if the gas “trickled in” at a lower rate or in several smaller events. Clearly, it is of interest to investigate constraints on star formation and feedback models stemming from this.

Understanding the evolution in profile shapes, in particular how central versus outer densities evolve, is necessary to constrain how the potential and binding energy at the centers of spheroids evolve. This may be intimately related to the BH-host galaxy correlations in feedback-regulated models of BH growth (see e.g. Hopkins et al. 2007b,a, and references therein). There has been

considerable debate regarding the state of the BH-host correlations at these redshifts: better understanding of spheroid cores that dictate the local potential depth is critical to inform theoretical models.

Current observations suggest that a large fraction of the high-density material in spheroids was assembled at early times. Although we have shown that it is possible to accommodate the mass in dense, high redshift cores in the elliptical population today, the observations suggest that of order half the massive cores of today’s massive ellipticals had to be in place by $z > 2$. Compare this to just $\sim 5\%$ of the total spheroid mass density in place at these redshifts, and $\sim 20\%$ of the massive galaxy ($> 10^{11} M_{\odot}$) density (Grazian et al. 2007; Pérez-González et al. 2008; Marchesini et al. 2008). In other words, it appears that the massive cores of today’s ellipticals assembled preferentially early. This is qualitatively consistent with models of dissipational formation, but in semi-analytic models explaining early massive elliptical formation is quantitatively quite challenging (see e.g. Bower et al. 2006; Fontana et al. 2006). The observations thus constrain not just the total assembly, but how this takes place – invoking early minor mergers or gas-poor processes, for example, might be able to account for the shape of the mass function, but would not explain the early formation of dense cores.

The observational comparison here favors models in which high-redshift compact galaxies are not destroyed (as has typically been concluded), but accrete or reveal previously “hidden” extended envelopes of low surface-brightness material. Their central densities remain, but with the appearance of low-density material, the effective radii and profile shapes quickly become comparable to massive galaxies today. If the high redshift systems genuinely do not have such low-density envelopes, the required evolution is only a factor $\sim 1.5 - 2$ growth in stellar mass from high redshifts to today. Indeed, dry mergers onto such massive, early-forming systems are cosmologically inevitable, and the mass growth requirements found here are consistent with the current stellar mass function constraints (Brown et al. 2008; Perez-Gonzalez et al. 2008). Moreover most dry mergers in such massive systems will be with later-forming, less massive and less dense systems, that are not expected to disrupt the dense cores, but will instead build up an envelope of lower surface density material.

6.3 Observational Tests and Future Prospects

Observed high-redshift systems require the presence of extended, low surface density envelopes to match the profiles of massive ellipticals today. It is quite possible that such envelopes are accreted in the intervening redshifts, as described above. However, Figure 6 highlights that the high-redshift observations should be interpreted with some caution: they do not extend to the very low densities where much of the low-surface density material resides. And even where observations detect light at relatively low surface brightness, the relevant S/N weighting means that the profile fits are primarily sensitive to the high-brightness central regions. As a result, there could be significant differences in the best-fit R_e from high-redshift observations, compared to deep low-redshift observations of analogous systems. At low stellar masses, where Sérsic indices tend to be low, there is no strong dependence on the depth of the observations. At higher masses, however, where outer Sérsic indices in local systems are large because of the presence of large stellar envelopes, the effect can be substantial. We find that very deep observations are required to obtain “converged” effective radii in fits to local massive ellipticals: $\sim 6 - 8$ mag in surface brightness depth relative to the PSF/seeing-convolved maximum brightness.

⁶ We exclude cases where the systems are gas-dominated from this discussion, as in these cases the relevant physics leads to qualitatively different behavior in mergers, and will not necessarily make spheroids at all (Robertson et al. 2006; Hopkins et al. 2009a,c).

Even with the deepest high-redshift samples ($\sim 3 - 4$ mag depth), we conclude that much of an outer envelope could be missed, and the inferred R_e from the best fit may be a factor $\sim 2 - 4$ smaller than what is obtained from the extremely deep local observations. Note that these results do not demonstrate that extended stellar envelopes are present around $z \gtrsim 2$ compact galaxies, but rather that they could be missed if present.

These effects do not arise solely because of the existence of stellar envelopes. If such systems were perfect Sérsic profiles, even high- n_s profiles with large envelopes, then the bias in R_e would be much smaller. However, high-mass galaxies are *not* perfect Sérsic profiles – deep observations of local galaxies find that they are fundamentally two-component systems. Fitting a single Sérsic index, while statistically a good fit over any limited dynamic range, is not acceptable over a sufficiently large dynamic range and yields a best-fit Sérsic index that depends on the dynamic range fitted (Figure 6). We stress that, because of this, the observations are not necessarily “wrong” in any physical sense: they are recovering a correct, unbiased description of the light profile where they can meaningfully sample it. What is at issue here is the interpretation of data based on the implicit assumption that spheroids are all described by single Sérsic index profiles that do not change shape with the dynamic range fitted and that can be extrapolated beyond the observed range. In massive galaxies in the local Universe, this is not the case. If massive ellipticals such as NGC 4552 were present at $z > 0.5$, full recovery of their envelopes would require observations $\sim 4 - 5$ mag deeper than the best presently available (Figure 6).

This has important consequences even at low redshifts. Recent studies have claimed that *most* of the apparent size-mass evolution in massive galaxies occurs at very low redshifts, a factor of $\sim 2 - 3$ change in sizes between $z = 0.1 - 0.3$, with the evolution from $z = 0.4 - 2$ restricted to a smaller factor $\sim 1.5 - 2$ (Bernardi 2009; Ferreras et al. 2009). Such extreme low-redshift evolution strongly suggests that the effect is related to the observed dynamic range and fitting: it is almost impossible to explain such a large change in the true stellar half-mass radius in any model. Independent constraints have clearly established that in this redshift range, there is almost no evolution in the stellar mass function of massive spheroids, nor is there significant evolution in the (uniformly old) stellar populations, or any significant stellar mass loss or new star formation given the old stellar population ages (Thomas et al. 2005; Nelan et al. 2005; Gallazzi et al. 2006; Masjedi et al. 2006; Borch et al. 2006; Jones et al. 2006). Likewise, there is no change in their kinematics or the fundamental plane relation in clusters or the field (Treu et al. 2005; di Serego Alighieri et al. 2005; van der Wel et al. 2005; van Dokkum & van der Marel 2007). Even the dark matter halos grow by only a tiny fraction over the redshift range of $z = 0.1$ to 0.3 (< 0.1 dex; almost all accreted at large radii). What do change over this redshift range, however, are the spatial resolution and effective surface brightness limits, and as a consequence the radial range of the profile sampled in observations. We find that the observations of rapid changes in the best-fit R_e at low redshifts can be accounted for by the biases summarized in Figure 6.

Our results demonstrate that constraints on the presence or absence of low-surface brightness material at low and high redshifts are critical to improving our understanding of elliptical galaxy formation. Either result would be of considerable interest. If it is not present, then mergers forming spheroids must initially be quite gas rich, and low density accreting material at high redshift rare, to avoid building too much envelope. And subsequent mergers would be constrained to build up this amount of mass in low-density ma-

terial, perhaps putting requirements on models for tidal destruction and minor mergers as well as later dry major mergers. If envelopes are instead present at high redshift, it strongly limits the amount of growth, accretion, and dry merging such systems can undergo at lower redshifts, and requires substantial low-density extended material in spheroid progenitors. It will also increase the stellar masses of these massive systems (by factor $\sim 1.5 - 2$), making the high-redshift mass function of massive galaxies even closer to that at low-redshifts (a challenge for all galaxy formation models). It would also more strongly constrain which low-redshift populations can be the descendants of high-redshift spheroids.

There are a number of observational means to study these possibilities. Most directly, observations can probe whether such material exists at high redshifts. Profile fitting is not the ideal mechanism for such studies, and it may be prohibitively expensive to construct full surface brightness profiles out to such low surface densities. If, however, a large fraction of the elliptical light is in an extended envelope, it should be possible to estimate that total light contribution from comparison of deep integrations of the total light/stellar mass in fixed *physical* annuli. Observations of major and minor dry merger rates offer complimentary constraints on how much material is added to these systems between high redshifts and today. In the local universe, studying the properties of these envelopes can inform models of their formation histories. For example, stellar population gradients and kinematics might reflect a more dramatic transition in properties if the envelopes form by late accretion onto earlier-forming cores. If the envelopes form early, they will be metal poor and have different α -element abundances compared to late-accreting disk/outer bulge material. Together, these observations offer promising avenues towards constraining these otherwise very observationally challenging, low-surface brightness components.

Throughout this paper, we have neglected several additional physical effects that might affect estimates of the stellar surface mass densities and effective radii of high-redshift ellipticals. For example, at low redshifts, stellar mass-to-light ratios are independent of radius to within $\sim 20\%$ in optical bands in massive ellipticals, which tend to be uniformly old and have weak color gradients (see e.g. Faber et al. 1989; Bender et al. 1993). However, given the observed stellar population gradients run backwards in time, or considering local recent merger remnants and/or simulations, the expectation is that this could be quite different at the high redshifts when the ellipticals formed (Schweizer 1996; Rothberg & Joseph 2004; Yamauchi & Goto 2005). The young, post-starburst population (ages $\lesssim 1 - 2$ Gyr) in the core has higher optical L/M_* , which can lead to a rest-frame B -band best-fit R_e that is a factor $\sim 1.5 - 2$ smaller than the stellar-mass R_e (or the B -band R_e observed when the system has aged and this effect vanishes). There may also be some bias in estimated stellar masses of systems at similar ages, owing to the uncertain contribution of AGB stars (Maraston 2005; Maraston et al. 2006). This is estimated to be a possible factor $\sim 1.2 - 1.4$ over-estimate of the high-redshift masses where high-quality optical photometry is available (Wuyts et al. 2007, 2009). We have conservatively ignored these effects, but if present they will strengthen most of our conclusions. To test for these effects, it is important to obtain deeper spectra and photometry, to test for the presence of blue cores and constrain the contribution of stellar populations of different ages (and stellar population gradients) in systems at intermediate and high redshifts.

ACKNOWLEDGMENTS

We thank Todd Thompson, Ignacio Trujillo, and Marijn Franx for helpful discussions. Support for PFH was provided by the Miller Institute for Basic Research in Science, University of California Berkeley. EQ is supported in part by NASA grant NNG06GI68G and the David and Lucile Packard Foundation.

REFERENCES

- Abraham, R. G., et al. 2007, *ApJ*, 669, 184
- Allen, P. D., Driver, S. P., Graham, A. W., Cameron, E., Liske, J., & de Propris, R. 2006, *MNRAS*, 371, 2
- Balcells, M., Graham, A. W., & Peletier, R. F. 2007a, *ApJ*, 665, 1084
- . 2007b, *ApJ*, 665, 1104
- Barnes, J. E., & Hernquist, L. 1996, *ApJ*, 471, 115
- Bell, E. F., McIntosh, D. H., Katz, N., & Weinberg, M. D. 2003, *ApJS*, 149, 289
- Bell, E. F., et al. 2006, *ApJ*, 640, 241
- Bender, R., Burstein, D., & Faber, S. M. 1993, *ApJ*, 411, 153
- Bernardi, M. 2009, *MNRAS*, in press, arXiv:0901.1318
- Bernardi, M., Hyde, J. B., Sheth, R. K., Miller, C. J., & Nichol, R. C. 2007, *AJ*, 133, 1741
- Borch, A., et al. 2006, *A&A*, 453, 869
- Bower, R. G., Benson, A. J., Malbon, R., Helly, J. C., Frenk, C. S., Baugh, C. M., Cole, S., & Lacey, C. G. 2006, *MNRAS*, 370, 645
- Boylan-Kolchin, M., Ma, C.-P., & Quataert, E. 2006, *MNRAS*, 369, 1081
- Brown, M. J. I., Zheng, Z., White, M., Dey, A., Jannuzi, B. T., Benson, A. J., Brand, K., Brodwin, M., & Croton, D. J. 2008, *ApJ*, 682, 937
- Buitrago, F., Trujillo, I., Conselice, C. J., Bouwens, R. J., Dickinson, M., & Yan, H. 2008, *ApJL*, in press
- Burkert, A., Naab, T., Johansson, P. H., & Jesseit, R. 2008, *ApJ*, 685, 897
- Chabrier, G. 2003, *PASP*, 115, 763
- Cimatti, A., et al. 2008, *A&A*, 482, 21
- Conroy, C., & Wechsler, R. H. 2008, *ApJ*, in press, arXiv:0805.3346 [astro-ph], 805
- Côté, P., et al. 2006, *ApJS*, 165, 57
- . 2007, *ApJ*, 671, 1456
- Cox, T. J., Dutta, S. N., Di Matteo, T., Hernquist, L., Hopkins, P. F., Robertson, B., & Springel, V. 2006, *ApJ*, 650, 791
- Daddi, E., et al. 2005, *ApJ*, 626, 680
- Damjanov, I., et al. 2008, *ApJ*, in press, arXiv:0807.1744 [astro-ph], 807
- di Serego Alighieri, S., et al. 2005, *A&A*, 442, 125
- Faber, S. M., Wegner, G., Burstein, D., Davies, R. L., Dressler, A., Lynden-Bell, D., & Terlevich, R. J. 1989, *ApJS*, 69, 763
- Ferguson, H. C., et al. 2004, *ApJL*, 600, L107
- Ferrarese, L., et al. 2006, *ApJS*, 164, 334
- Ferreras, I., Lisker, T., Pasquali, A., Khochfar, S., & Kaviraj, S. 2009, *ApJ*, in press, arXiv:0901.4555
- Fontana, A., et al. 2006, *A&A*, 459, 745
- Franx, M., van Dokkum, P. G., Schreiber, N. M. F., Wuyts, S., Labbé, I., & Toft, S. 2008, *ApJ*, 688, 770
- Gallagher, III, J. S., & Ostriker, J. P. 1972, *AJ*, 77, 288
- Gallazzi, A., Charlot, S., Brinchmann, J., & White, S. D. M. 2006, *MNRAS*, 370, 1106
- Graves, J., et al. 2009, *ApJ*, in preparation
- Grazian, A., et al. 2007, *A&A*, 465, 393
- Hausman, M. A., & Ostriker, J. P. 1978, *ApJ*, 224, 320
- Hernquist, L., Spergel, D. N., & Heyl, J. S. 1993, *ApJ*, 416, 415
- Hibbard, J. E., & Yun, M. S. 1999, *ApJL*, 522, L93
- Hopkins, P. F., Cox, T. J., Dutta, S. N., Hernquist, L., Kormendy, J., & Lauer, T. R. 2008a, *ApJ*, accepted, arXiv:0805.3533 [astro-ph], 805
- Hopkins, P. F., Cox, T. J., & Hernquist, L. 2008b, *ApJ*, 689, 17
- Hopkins, P. F., Cox, T. J., Younger, J. D., & Hernquist, L. 2009a, *ApJ*, 691, 1168
- Hopkins, P. F., Hernquist, L., Cox, T. J., Dutta, S. N., & Rothberg, B. 2008c, *ApJ*, 679, 156
- Hopkins, P. F., Hernquist, L., Cox, T. J., Kereš, D., & Wuyts, S. 2009b, *ApJ*, 691, 1424
- Hopkins, P. F., Hernquist, L., Cox, T. J., Robertson, B., & Krause, E. 2007a, *ApJ*, 669, 45
- . 2007b, *ApJ*, 669, 67
- Hopkins, P. F., Lauer, T. R., Cox, T. J., Hernquist, L., & Kormendy, J. 2008d, *ApJ*, in press, arXiv:0806.2325 [astro-ph], 806
- Hopkins, P. F., Lidz, A., Hernquist, L., Coil, A. L., Myers, A. D., Cox, T. J., & Spergel, D. N. 2007c, *ApJ*, 662, 110
- Hopkins, P. F., Somerville, R. S., Cox, T. J., Hernquist, L., Jogee, S., Kereš, D., Ma, C.-P., Robertson, B., & Stewart, K. 2009c, *MNRAS*, in press, arXiv:0901.4111 [astro-ph]
- Hopkins, P. F., et al. 2009d, *ApJ*, in preparation
- Jesseit, R., Naab, T., Peletier, R. F., & Burkert, A. 2007, *MNRAS*, 376, 997
- Jones, D. H., Peterson, B. A., Colless, M., & Saunders, W. 2006, *MNRAS*, 369, 25
- Kennicutt, Jr., R. C. 1998, *ApJ*, 498, 541
- Khochfar, S., & Silk, J. 2006, *ApJL*, 648, L21
- Komatsu, E., et al. 2008, *ApJ*, in press, arXiv:0803.0547 [astro-ph], 803
- Kormendy, J. 1999, in *Astronomical Society of the Pacific Conference Series*, Vol. 182, *Galaxy Dynamics - A Rutgers Symposium*, ed. D. R. Merritt, M. Valluri, & J. A. Sellwood, 124–+
- Kormendy, J., Fisher, D. B., Cornell, M. E., & Bender, R. 2008, *ApJ*, in press, arXiv:0810.1681 [astro-ph]
- Kriek, M., van der Wel, A., van Dokkum, P. G., Franx, M., & Illingworth, G. D. 2008a, *ApJ*, 682, 896
- Kriek, M., et al. 2006, *ApJL*, 649, L71
- . 2008b, *ApJ*, 677, 219
- Labbé, I., et al. 2005, *ApJL*, 624, L81
- Lauer, T. R., et al. 2007, *ApJ*, 664, 226
- Lin, L., et al. 2008, *ApJ*, 681, 232
- Maraston, C. 2005, *MNRAS*, 362, 799
- Maraston, C., Daddi, E., Renzini, A., Cimatti, A., Dickinson, M., Papovich, C., Pasquali, A., & Pirzkal, N. 2006, *ApJ*, 652, 85
- Marchesini, D., van Dokkum, P. G., Forster Schreiber, N. M., Franx, M., Labbé, I., & Wuyts, S. 2008, *ApJ*, in press, arXiv:0811.1773 [astro-ph]
- Masjedi, M., et al. 2006, *ApJ*, 644, 54
- McIntosh, D. H., et al. 2005, *ApJ*, 632, 191
- Mihos, J. C., & Hernquist, L. 1994, *ApJL*, 437, L47
- Naab, T., Jesseit, R., & Burkert, A. 2006, *MNRAS*, 372, 839
- Naab, T., Johansson, P. H., Ostriker, J. P., & Efstathiou, G. 2007, *ApJ*, 658, 710
- Nelan, J. E., et al. 2005, *ApJ*, 632, 137
- Oñorbe, J., Domínguez-Tenreiro, R., Sáiz, A., Artal, H., & Serna, A. 2006, *MNRAS*, 373, 503
- Ostriker, J. P., & Tremaine, S. D. 1975, *ApJL*, 202, L113
- Perez-Gonzalez, P. G., Trujillo, I., Barro, G., Gallego, J., Zamorano, J., & Conselice, C. J. 2008, *ApJ*, in press, arXiv:0807.1069 [astro-ph], 807

- Pérez-González, P. G., et al. 2008, *ApJ*, 675, 234
- Quadri, R., et al. 2007, *ApJ*, 654, 138
- Ravindranath, S., et al. 2004, *ApJL*, 604, L9
- Robertson, B., Bullock, J. S., Cox, T. J., Di Matteo, T., Hernquist, L., Springel, V., & Yoshida, N. 2006, *ApJ*, 645, 986
- Rothberg, B., & Joseph, R. D. 2004, *AJ*, 128, 2098
- Sánchez-Blázquez, P., Forbes, D. A., Strader, J., Brodie, J., & Proctor, R. 2007, *MNRAS*, 377, 759
- Schweizer, F. 1996, *AJ*, 111, 109
- Shapiro, K. L., et al. 2008, *ApJ*, 682, 231
- Shen, S., Mo, H. J., White, S. D. M., Blanton, M. R., Kauffmann, G., Voges, W., Brinkmann, J., & Csabai, I. 2003, *MNRAS*, 343, 978
- Somerville, R. S., et al. 2008, *ApJ*, 672, 776
- Tacconi, L. J., Neri, R., Chapman, S. C., Genzel, R., Smail, I., Ivison, R. J., Bertoldi, F., Blain, A., Cox, P., Greve, T., & Omont, A. 2006, *ApJ*, 640, 228
- Tacconi, L. J., et al. 2008, *ApJ*, 680, 246
- Thomas, D., Maraston, C., Bender, R., & Mendes de Oliveira, C. 2005, *ApJ*, 621, 673
- Thompson, T. A., Quataert, E., & Murray, N. 2005, *ApJ*, 630, 167
- Toft, S., et al. 2007, *ApJ*, 671, 285
- Trager, S. C., Faber, S. M., Worthey, G., & González, J. J. 2000, *AJ*, 119, 1645
- Treu, T., et al. 2005, *ApJ*, 633, 174
- Trujillo, I., Asensio Ramos, A., Rubiño-Martín, J. A., Graham, A. W., Aguerri, J. A. L., Cepa, J., & Gutiérrez, C. M. 2002, *MNRAS*, 333, 510
- Trujillo, I., Cenarro, A. J., de Lorenzo-Caceres, A., Vazdekis, A., de la Rosa, I. G., & Cava, A. 2009, *ApJL*, in press, arXiv:0901.1032
- Trujillo, I., Conselice, C. J., Bundy, K., Cooper, M. C., Eisenhardt, P., & Ellis, R. S. 2007, *MNRAS*, 382, 109
- Trujillo, I., et al. 2004, *ApJ*, 604, 521
- . 2006a, *MNRAS*, 373, L36
- . 2006b, *ApJ*, 650, 18
- van der Wel, A., Franx, M., van Dokkum, P. G., Rix, H.-W., Illingworth, G. D., & Rosati, P. 2005, *ApJ*, 631, 145
- van der Wel, A., Holden, B. P., Zirm, A. W., Franx, M., Rettura, A., Illingworth, G. D., & Ford, H. C. 2008, *ApJ*, 688, 48
- van Dokkum, P., et al. 2008, *ApJL*, 677, L5
- van Dokkum, P. G. 2005, *AJ*, 130, 2647
- van Dokkum, P. G., & van der Marel, R. P. 2007, *ApJ*, 655, 30
- van Dokkum, P. G., et al. 2006, *ApJL*, 638, L59
- Weil, M. L., & Hernquist, L. 1994, *ApJL*, 431, L79
- . 1996, *ApJ*, 460, 101
- Wuyts, S., Franx, M., Cox, T. J., Hernquist, L., Hopkins, P. F., Robertson, B. E., & van Dokkum, P. G. 2009, *ApJ*, in press, arXiv:0901.4337
- Wuyts, S., et al. 2007, *ApJ*, 655, 51
- Yamauchi, C., & Goto, T. 2005, *MNRAS*, 359, 1557
- Younger, J. D., et al. 2007, *ApJ*, 671, 1531
- . 2008, *ApJ*, 688, 59
- Zheng, Z., Coil, A. L., & Zehavi, I. 2007, *ApJ*, 667, 760
- Zirm, A. W., et al. 2007, *ApJ*, 656, 66